WARSAW UNIVERSITY OF TECHNOLOGY Index 351733
FACULTY OF CIVIL ENGINEERING
COMMITTEE FOR CIVIL AND WATER ENGINEERING
POLISH ACADEMY OF SCIENCES ISSN 1230-2945
DOI: 10.24425/ace.2024.151885
ARCHIVES OF CIVIL ENGINEERING
Vol. LXX ISSUE 4 2024
pp. 149–162

Research paper

Vision-based experimental study of force estimation in the cable-stayed bridge's cable model

Yanhao Li[1], Mustafasanie M. Yussof[2], Xing Tan[3], Shicai Yuan[4]

Abstract: In this paper, a vision-based measurement is proposed, so as to realize quick and convenient tests on the cable force of single-cable plane cable-stayed bridge. Firstly, laser is used to lay out the reference points, and pictures are taken by mobile phone or camera, gaining cable sag by serial image processing. The next step is to calculate the cable force by its relation with sag. According to laboratory test of cable force, the measuring error of cable force is within 3%, which meets the engineering precision requirements. This simple, efficient and low-risk method is easy to operate, and can solve the difficulty of marker installation during visual measurement.

Keywords: bridge monitoring, cable force estimation, image perspective transformation, laser target, sag

[1]MsC., School of Civil Engineering, Universiti Sains Malaysia, Engineering Campus, 14300 Nibong Tebal, Pulau Pinang, Malaysia; School of Civil and Architectural Engineering, Yangtze Normal University, Chongqing 408100, China, e-mail: li.yanhao@student.usm.my, ORCID: 0009-0008-5797-892X

[2]PhD., School of Civil Engineering, Universiti Sains Malaysia, Engineering Campus, 14300 Nibong Tebal, Pulau Pinang, Malaysia, e-mail: cemustafa@usm.my, ORCID: 0000-0002-3563-5466

[3]PhD., School of Civil and Architectural Engineering, Yangtze Normal University, Chongqing 408100, China, e-mail: 531721411@qq.com, ORCID: 0000-0003-3140-9901

[4]MsC., School of Civil and Architectural Engineering, Yangtze Normal University, Chongqing 408100, China, e-mail: yuanshicai@yznu.edu.cn ORCID: 0009-0005-1293-039X

1. Introduction

Cable tension in cable-stayed bridges is a focal point of attention during both bridge construction and operational phases [1]. Existing tension force testing methods exhibit the following characteristics [2–6].

The hydraulic gauge method is primarily utilized during the installation or replacement of cables. The pressure sensor method involves installing pressure sensors at the cable ends, but due to concerns regarding stability and cost, it is unsuitable for long-term monitoring. The electromagnetic method requires establishing a relationship curve between tension force, temperature, magnetic field intensity, and permeability, making it challenging to ensure the stability and reliability of test results. While the traditional frequency method is widely applied, its efficiency is low, and test results are significantly influenced by the main beam and dampers. The cable shape method faces limitations in generalization due to insufficient precision of total stations or the high cost of 3D laser scanners [7, 8].

In recent years, visual-based methods have seen increasing application in structural monitoring [9–12]. Affixing markers to the cables, using a total station to measure marker coordinates, and performing image perspective transformation allows for the estimation of cable tension based on cable plane shapes [13]. Recording cable videos and employing image matching methods to obtain cable vibration frequencies also enable tension force estimation [14]. The accuracy of tension force testing often correlates with the pixel resolution of the camera. Studies indicate that even with inexpensive, low-resolution cameras, cable tension estimation can be achieved through high-speed recording [15]. Furthermore, while catenary theory provides high precision in estimating tension force, in practice, the accuracy corresponding to parabolic theory still meets engineering requirements [16–18].

In the case of most double-plane or multi-plane cable-stayed bridges, the cables are symmetrically arranged about the centerline of the bridge deck, resulting in overlapping projections of the cables in the vertical plane. This overlapping scenario complicates the accurate determination of the shape of each cable [19]. However, single-plane cable-stayed bridges typically position the inclined cables within the same vertical plane corresponding to the centerline of the bridge deck. Therefore, obtaining the projection of the bridge in the vertical plane allows for the determination of the cable plane shapes [20]. Fig. 1 shows typical cable-stayed bridges with single cable plane or three cable planes.

Fig. 1. Pictures of cable-stayed bridges

For the reasons outlined above, this paper proposes a vision-based tension force estimation method tailored for single-plane cable-stayed bridges, subsequently validated through experimentation. Derived from the cable shape method, the approach primarily utilizes common photographic equipment such as smartphones or cameras for capturing images of the bridge. Employing a laser emitter with markers, the method involves a series of techniques, including image perspective transformation, to obtain the cable shapes, followed by the inverse calculation of tension forces. This method maintains the theoretical advantages akin to the cable shape method while offering flexibility, efficiency, low cost, and minimal risk.

2. Measurement principles

2.1. The relationship between cable sag and cable force

Ernst proposed the basic theory of the relationship between the sag and the cable force in 1965 [14]. In this study, the influence of bending stiffness and gravity on the direction component of the cable is ignored. The stay cable is regarded as a simply supported beam. The force diagram of the cable is shown in Fig. 2. What's more, the cable curve is a quadratic parabola, and the mid-span bending moment is zero, with the force diagram of half cable shown in Fig. 2(c).

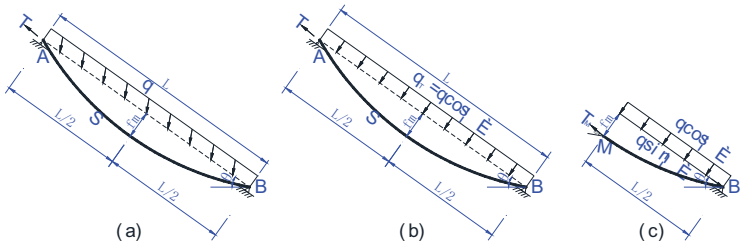

Fig. 2. Diagram of cable tension: (a) Entirety, (b) Vertical component of gravity extension, (c) Half for the lower endpoint (point B)

A moment line equilibrium formula is as follows Eq. (2.1),

$$T_M f_m = \frac{1}{8} q L^2 \cos\theta \tag{2.1}$$

where, q is the gravity concentration of the cable, f_m is the radial deflection (sag) in the span of the cable, and θ is the horizontal dip Angle of the cable.

Assuming that the cable force at the middle point is T_M, the bottom cable force is T_0 and the top cable force is T_L. So we can get Eq. (2.2),

$$\begin{cases} T_M = \dfrac{qL^2}{8 f_m} \cos\theta \\ T_o = T_M - 0.5 L q \sin\theta \\ T_L = T_M + 0.5 L q \sin\theta \end{cases} \tag{2.2}$$

Therefore, the key of cable force testing method based on cable shape is to obtain the accurate sag f_m of cable at the mid-span position.

2.2. Camera calibration

The camera may introduce distortions in photos due to lens manufacturing errors and other factors. Common distortions include pillow distortion (Fig. 3b) and barrel distortion (Fig. 3c). In this study, camera calibration is essential. Zhang's method [21] is a commonly used and mature calibration approach. This method has readily available toolboxes in MATLAB for direct utilization. Fig. 4 presents the calibration results for the mobile phone camera.

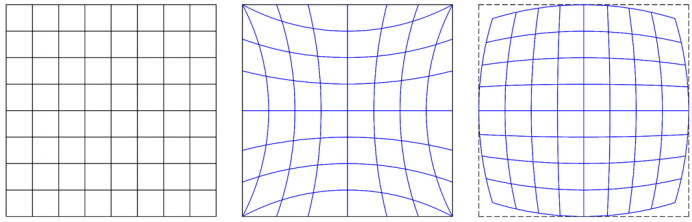

(a) (b) (c)

Fig. 3. Image distortion diagram: (a) normal image, (b) Occipital distortion, (c) Bucket distortion

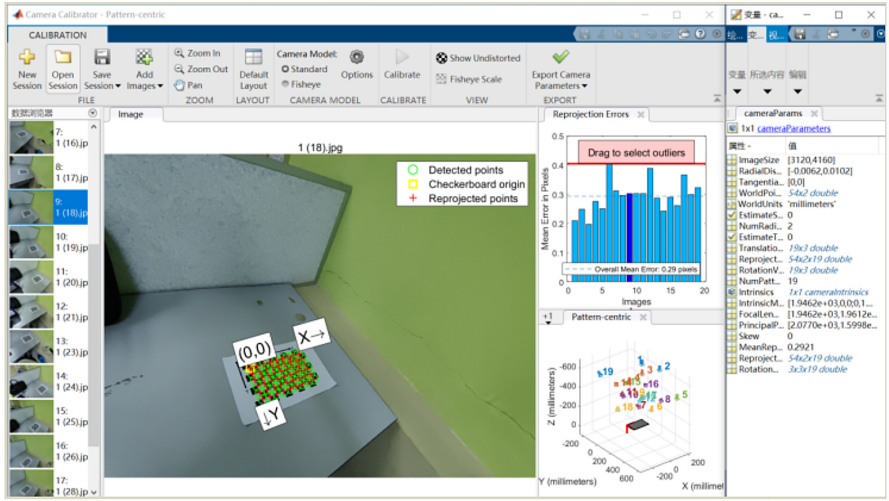

Fig. 4. Result of camera calibration

2.3. Image perspective transformation

Under the combined influence of its self-weight and tension force, the cable forms a planar curve. Consequently, it is possible to obtain an orthographic projection photograph of the cable to determine its sag. However, it is evident that the camera introduces both horizontal and vertical angles during capture, resulting in an image that is "larger up close and smaller from a distance", commonly known as "perspective". In Fig. 5a, L2 is noticeably larger than L1.

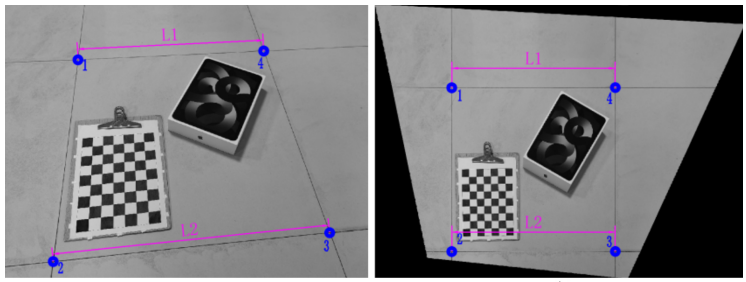

(a) (b)

Fig. 5. Image perspective transformation: (a) Original image, (b) Transformed image

Perspective transformation can obtain the front projection of the photo taken with oblique axis. The logic behind is to project the captured image onto a new visual plane, with its general transformation formula shown in Eq. (2.3).

$$\begin{bmatrix} X \\ Y \\ Z \end{bmatrix} = \begin{bmatrix} a_{11} & a_{12} & a_{13} \\ a_{21} & a_{22} & a_{23} \\ a_{31} & a_{32} & a_{33} \end{bmatrix} \begin{bmatrix} x \\ y \\ z \end{bmatrix} = T \begin{bmatrix} x \\ y \\ z \end{bmatrix} \tag{2.3}$$

T is called the perspective transformation matrix. (x, y, z) is the homogeneous coordinates of pixels in the original image, and (X, Y, Z) is the homogeneous coordinates of the image pixels after transformation. Where $Z = 1$, (X, Y) is the plane coordinate of the pixel corresponding to the original image after transformation.

As shown in Eq. (2.3), the transformation matrix has 9 unknowns, but with only 8 degrees of freedom. So there are actually eight unknowns. The camera attitude is unknown when shooting. Together, it is very difficult to obtain the 8 parameters in the transformation matrix through the geometric relationship between the camera and the subject. Therefore, control point method is often introduced to complete perspective transformation of image in engineering.

The function for this method in MATLAB is “Imtransform”. Fig. 5b illustrates the comparative effect after perspective transformation of Fig. 5a. It is crucial to note that, for more accurate perspective transformation results, the four points selected should be positioned as close as possible to the four corners of the image. In Fig. 5b, the number of pixels occupied by identical sizes at any position in both xy directions is the same ($L1 = L2$). Therefore, for tension force estimation, once the image undergoes perspective transformation, pixel ratio calibration and cable sag measurement can be conducted.

2.4. Image interpolation operation

Perspective transformation is an image geometry operation. During this process, the position of pixel coordinates after transformation is often non-integer ones. Since digital images only record integers, the position needs to be rounded and then the gray value is redistributed to integer coordinates, namely the image interpolation operation. Most popular interpolation methods include nearest, bilinear and bicubic ones.

Fig. 6 shows the comparison graph obtained by using the above-mentioned three interpolation methods to amplify Lena by five times from original 512×512. A 450-by-450 image near the eye was then taken for comparison.

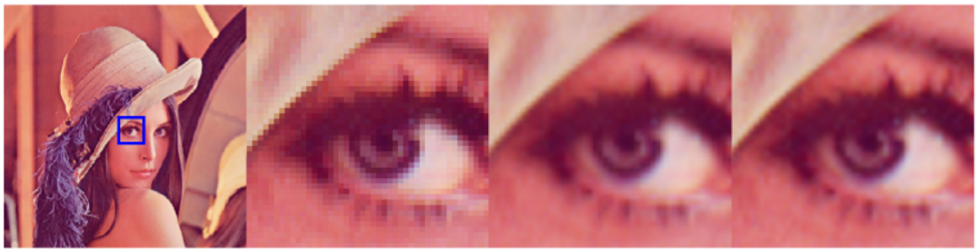

(a) (b) (c) (d)

Fig. 6. Comparison of the effects of different interpolation functions: (a) original image, (b) nearest, (c) bilinear, (d) bicubic

As shown in Fig. 6, after enlarged by 10 times, there are obvious square pixels in (b), obvious jagged pixels in the position of gray value mutation, with rough edges. The effects of (c) and (d) are similar without obvious square pixels. In fact, if the original image is enlarged to a larger multiple, the double cubic difference can save the image details better. Due to limited space, here is no further relevant display. Therefore, the binary cubic interpolation method is selected for interpolation processing.

2.5. Image contour extraction

So far, many scholars have conducted systematic researches on image edge extraction, with some mature algorithms including Sobel operator, Prewitt operator and Canny operator. Based on these algorithms, corresponding optimized versions are developed for different scenarios. Clearly, operators vary in features. Although the Canny operator works well for edge detection in any direction, its parameter setting and computation are very large. In engineering, the background of the stay cable is mostly the sky, so the gray level of the image is obviously different. Therefore, operators with small computation and good adaptability should be selected. In this paper, Sobel operator function in Matlab is chosen for edge detection, and the cable contour is extracted.

3. Methodology for measurement

Based on the static image, the specific steps for force estimation include: setting the reference target point, measuring the target point coordinates, image correction and perspective transformation, obtaining the shape and sag of the cable, and finally calculating the tension force by reverse calculation of the sag.

3.1. Obtain base point coordinates and images

1. Set the laser target
   Due to the large dimensions of the bridge, manual installation of target points is often impractical in many locations. Therefore, one can employ a laser emitter to generate target points within the cable plane, facilitating the acquisition of perspective transformation reference point information. Given the characteristics of a single cable surface inclined cable-stayed bridge, a set of four non-collinear target points can be established in a single instance, capturing the shape of all cables in a single photograph. Considering the relatively small diameter of the cables in relation to the measuring distance, achieving precise alignment with the laser proves challenging. Fixing the laser emitter on a leveling instrument and utilizing the instrument's fine adjustment knob can aid in achieving accurate alignment.
2. Get the reference point coordinates
   Following the establishment of laser target points, the total station is employed to measure these points. Concerning perspective transformation, it suffices to ascertain the relative positions of the four reference points within the plane. Therefore, the total station only requires leveling, devoid of any need for known points in a specific coordinate system as references. Once the coordinates of the total station stationing point are set (which can be arbitrarily chosen), the relative distances between the four reference points can be directly measured using a prismless method.
3. Acquire image
   Finishing the previous step, the camera shoots the target object. If conditions permit, the vertical and horizontal dip angles of the camera should be reduced as far as possible. That is, the photographic axis should be as perpendicular to the vertical plane where the cable is located, and the shooting target should be filled as far as possible to achieve a higher pixel rate.

3.2. Image-based cable force estimation

After obtaining the cable image, the camera calibration data with the same focal length is adopted to correct the image distortion. Then the image perspective transformation is conducted by the method in section 2.3, so as to obtain the orthographic projection image of the cable plane.

The core aspect of tension force testing based on image processing is to obtain the planar shape of the cable. Clearly, directly obtaining the central curve through 2D images is complex and is constrained by the grayscale values on the cable surface (due to surface dust or water marks). Since the rotational radius of the cable is sufficiently large compared to its diameter, selecting the edge curve of the cable as a substitute for the central curve is a viable option.

In particular, the corresponding sag calculation of the cable's lower edge is taken as an example. After obtaining the edge of the cable shape, the pixel coordinates (x_1, y_1) and (x_3, y_3) of the high point P1 and the low point P3 of the cable are firstly determined, then the pixel coordinates of P2 near the midpoint of the cable $((x_1 + x_3)/2, y_2)$. The x-direction coordinate of point P2 is calculated by $x_2 = (x_1 + x_3)/2$. The y-direction coordinate needs to be read

in the image. As shown in Fig. 7, the deformation caused by the cable's self-weight is very small compared to the cable length. In the figure, the β angle tends to 90°. Therefore, the approximate formula for calculating the sag of the cable is Eq. (3.1):

$$f \approx d\cos\alpha = \left(y_2 - \frac{y_1 + y_3}{2}\right)\cos\alpha \tag{3.1}$$

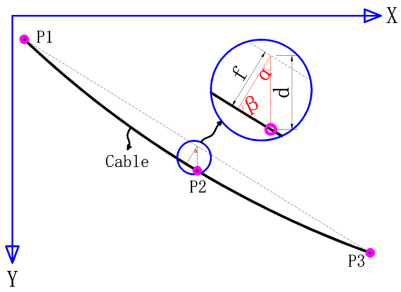

Fig. 7. Vertical calculation diagram

At this point, the sag value is measured in pixels. The reference point's relevant coordinates can be utilized to determine the image pixel rate (the length of the world coordinate system represented by each pixel in the image). In this aspect, Eq. (3.2) is for calculating pixel rate. After getting the cable sag, Eq. (2.2) is used to estimate the cable force.

$$k = \left[\frac{\text{mm}}{\text{pixel}}\right] = \frac{L}{l} = \frac{L_{ij}}{\sqrt{(x_i - x_j)^2 + (y_i - y_j)^2}}, \quad (i = 1 \text{ to } 4, j = 1 \text{ to } 4, i \neq j) \tag{3.2}$$

L_{ij} is the true distance between any two reference points.

4. Verification by laboratory experiment

4.1. Experimental model and parameter design

The lasso model experiment aims to verify whether the test method is feasible and accurate in this paper. As shown in Fig. 8, the experimental cable is installed, and the cable's lower end of is anchored to the railing post. The upper end bypasses the fixed pulley and lowers the weight to adjust the cable tension. After installing the force gauge at the anchorage position at the lower end of the model, the real tension of cable anchorage end can be finally obtained.

The cable adopts a single wire rope of "6 × 19+IWS", with its diameter of about 6 mm, and the linear density of 0.1392 kg/m. According to the similarity theory, the model should meet the similarity in geometric size, elastic modulus, load and other aspects. Therefore, after determining the section and elastic modulus of the experimental cable, other model parameters are determined according to the cable information of an actual bridge in Chongqing, China. Particularly, the selected similarity index is geometric size and load ratio. As shown in Fig. 9

with the reference bridge elevation diagram in this study, the information about the three-stay cables. The info, including cable dip angle, cable length and number of cable components. In this study, the outermost LA10 cable was selected for simulation.

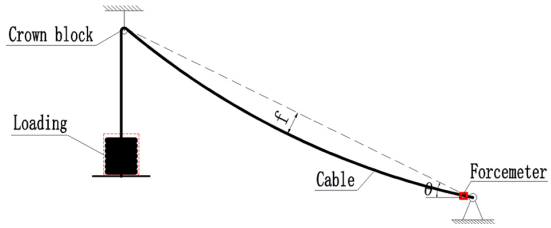

Fig. 8. Installation diagram of cable model

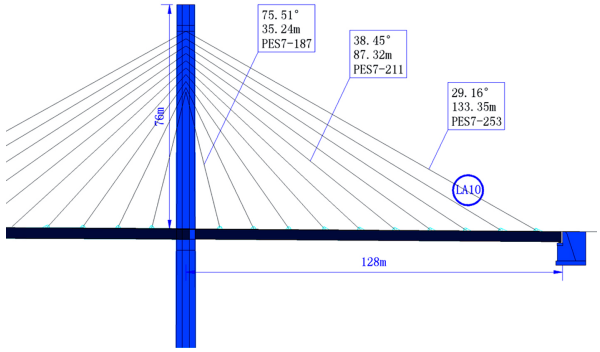

Fig. 9. References to the bridge's partial elevation

The parameter comparisons between the prototype cable and the model one is shown in Table 1. The prototype parameters in the table have same construction data of the real bridge. The elastic modulus of the model cable is measured by laboratory tensile test.

Table 1. Parameter comparison table between model cable and prototype cable

Cable style	**Sectional area A (mm^2)**	**Theoretical cable force T (kN)**	**Elasticity modulus E (GPa)**	**Geometric scale ratio**	**Linear density p (kg/m)**	**Load-to-weight ratio T/p**	**Cable length L (m)**
Model	17.55	£¿	98.55	14.98	0.1392	4.0579	8.90
Prototype	9736.5	4646.1	200.00	–	76.432	60.7874	133.35

As shown in Table 1, the geometric scale of the fabricated model cable is 1:14.98, and the ratio of cable force to linear density of the prototype cable is 60.7874. Therefore, the cable force required by the model cable is calculated as shown in Eq. (4.1).

$$T_{\text{mod}} = \frac{\rho_{\text{mod}}}{\lambda} \times \frac{T_{\text{r}}}{\rho_{\text{r}}} = \frac{0.1392}{14.98} \times \frac{4646.1}{76.432} \approx 0.565 \text{ kN} \tag{4.1}$$

In order to facilitate weight loading and compare multiple sets of data, weights in the experiments were applied ranging from 40 kg to 80 kg, adding by 10 kg each time. The tension force readings at the lower end of the cable corresponding to various load levels are 386.51 N, 485.60 N, 579.77 N, 676.89 N, and 772.05 N, respectively.

In order to better simulate the cable boundary conditions, after getting cable force readings at different load levels, the formal experiment is carried out without the rigometer. The experimental site layout and the markers are shown in Fig. 10.

Fig. 10. Experimental site layout and the markers

4.2. Experimental process

1. Image acquisition
   In this experiment, 4 reference points were set in the vertical plane where the cable was located. To this end, two of the points are arranged on the cable of the measuring section, one point on the cable behind the fixed pulley, and the last on the vertical line attached to the cable. The laser points and marked target points are illustrated in Fig. 10.
   Considering small cable diameter, the laser emitter is fixed on the level in this study, so as to align the laser cable with the fine tuning function, which is realized by the fine-tuning knob of the level. The experimental site layout is shown in Fig. 10. The positions of laser transmitter and total station are placed randomly in the figure, and camera position is only for schematic position.
   A total of five levels of loading are set and 10 minutes of waiting time are given after each stage is loaded. When the wire rope is stable without obvious vibration, laser alignment is initiated, then the spatial coordinates of the four reference points were measured. Finally, the wire rope is photographed. To be noted, all parts of the cable should be included in the image.
   In this experiment, Huawei P50 mobile phone was used for shooting with high pixel mode. The image pixel size is 8192×6144 at fixed focal length equivalent to 27 mm. Aperture value is f/1.8.
   Fig. 11 shows Original images and corrected images with loads of 40 kg.

(a) (b)

Fig. 11. Original images and Corrected images: (a) Original, (b) Corrected

2. Image processing
   The images treated with perspective transformation by the method in Section 2.3 are shown Fig. 11(b). With limited space, only the processed images corresponding to the load mass of 40 kg will be displayed afterwards. In this paper, Sobel Operator is used for edge detection [22]. Fig. 12 shows the whole cable edge image and its details.

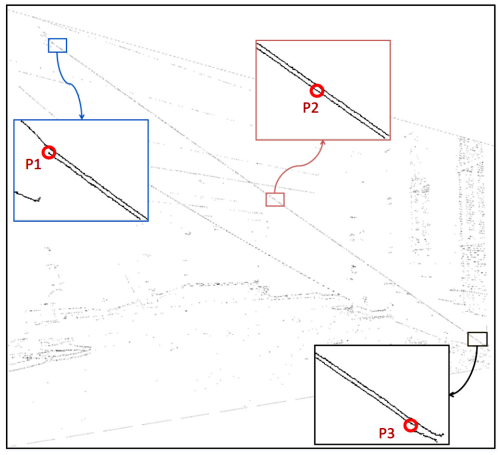

Fig. 12. Cable edge extraction image

4.3. Experimental results and analysis

The test results with 5 grade of loads in the experiment are shown in Table 2. Fig. 13 shows the comparisons between the tested and real values of cable force under different loads.

The experimental results show that the different load peso force models can be obtained by changing the cable force. The absolute errors of the measured cable forces are all within 3%, and the error rate can be positive or negative. The experimental errors mainly come from:

1. Cable vibration: The reference point's coordinate measurement and image shooting were carried out 10 minutes after completing loading. Even the indoor condition cannot avoid cable vibration. Therefore, there are naturally some differences between the actual cable position and the ideal one in the image.
2. Coordinate measurement: there is some error in measuring data point coordinates with total station instrument, mainly human and instrument errors. For example, the optical center of the total station is not completely aligned with the laser marker.
3. Image processing: such errors may happen during image distortion correction, perspective transformation or edge extraction. Moreover, distortion correction is related to camera calibration accuracy, perspective transformation to the precision of obtaining reference point coordinates before and after image transformation, and edge extraction to image processing algorithm.

Table 2. Experimental results

Loading level	Weight mass [kg]	Sag [mm]	Measuring cable length [mm]	Angle [°]	Evaluated tension [kN]	True tension [kN]	Error rate [%]
1	40	29.22	8911	34.99	0.3766	0.3865	–2.57
2	50	22.43	8911		0.4916	0.4856	1.24
3	60	19.61	8909		0.5625	0.5798	–2.98
4	70	15.88	8908		0.6953	0.6769	2.72
5	80	13.92	8908		0.7937	0.7711	2.94

Note: The gravitational acceleration is 9.81N/kg.
The error rate is: (measured cable force-cable force true value)/cable force true value ×100%.

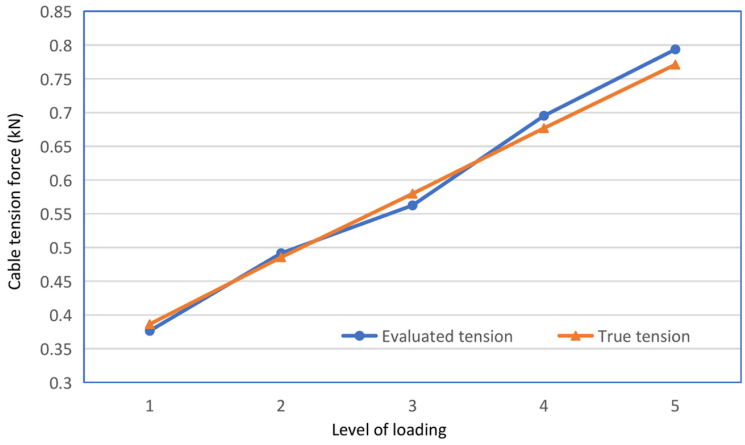

Fig. 13. Comparison diagram of cable force measured value and cable force

5. Conclusions

This paper presents a cable force measurement for single-cable plane cable-stayed bridges, mainly based on the cable layout characteristics of this bridge type. In addition, a method of obtaining reference point target by laser irradiation is proposed. The cable's plane shape is obtained by using perspective transformation. Then the cable force is evaluated based on the cable form method. Finally, this method is verified by laboratory experiments.

This study draws the following conclusions.

1. The laser irradiation method can effectively obtain the data point marker against the common problem of marker installation in practical engineering. By attaching the laser to the level, fast alignment can be realized.
2. Each image only needs 4 data points to estimate the cable force of multiple cables. With high enough pixel rate, only one image is necessary to estimate all the cable forces of the whole bridge.
3. The cable force estimation formula based on parabola theory can meet the accuracy requirements of actual engineering. Moreover, the upper edge or lower edge lines instead of the center line are feasible to estimate the cable force.
4. Slight cable vibration in outdoor bridge testing is a problem, which can be solved by taking multiple photos in a short time and averaging them. At present, the shooting speed of ordinary cameras can fully meet the needs.

To sum up, the method based on cable shape, laser target and image perspective transformation is adopted, which is a simple, efficient, convenient and low-risk way to estimate the cable force of single-cable plane cable-stayed bridges. The efficiency of the proposed method is fully proved by theory discussions and experiments. However, the accuracy of this method remains to be further verified by practical case of large field of view and complex terrain environment for outdoor solid bridges.

Acknowledgements

This research was supported by the Science and Technology Research Program of Chongqing Municipal Education Commission (Grant No.: KJQN202301434) and Chongqing Fuling Science and Technology Bureau (Grant No.: FLKJ2023AAG1025).

References

[1] L. Zhang, G. Qiu, and Z. Chen, "Structural health monitoring methods of cables in cable-stayed bridge: A review", *Measurement*, vol. 168, art. no. 108343, 2021, doi: 10.1016/j.measurement.2020.108343.

[2] J. Dai, F. Qin, J. Di, and Y. Chen, "Review of cable force optimization method for cable-stayed bridge in completed bridge state", *China Journal of Highway and Transport*, vol. 32, no. 5, pp. 17–37, 2019, doi: 10.19721/j.cnki.1001-7372.2019.05.002.

[3] Y.F. Duan, R. Zhang, C.Z. Dong, and Y.Z. Luo, "Development of elasto-electric (EME) sensor for in-service cable force monitoring", *International Journal of Structural Stability and Dynamics*, vol. 16, no. 4, art. no. 1640016, 2016, doi: 10.1142/S0219455416400162.

[4] J.W. Kim and S. Park, "Magnetic flux leakage sensing and artificial neural network pattern recognition-based automated damage detection and quantification for wire rope non-destructive evaluation", *Sensors*, vol. 18, no. 1, art. no. 109, 2018, doi: 10.3390/s18010109.

[5] Y. Zhou, P. An, J. Cao, J. Zhang, and C. Liu, "Design of by-pass excitation cable force sensor", *Journal of Physics: Conference Series*, vol. 1267, no. 1, art. no. 012068, 2019, doi: 10.1088/1742-6596/1267/1/012068.

[6] G.D. Zhou,and T.H. Yi, "A summary review of correlations between temperatures and vibration properties of long-span bridges", *Mathematical Problems in Engineering*, vol. 2014, no. 1, 2014, doi: 10.1155/2014/638209.

[7] Y. Zhou, Z. Huang, Y. Wang, Z. F. Xiang, J.T. Zhou, and X.S. Zhang, "Measurement method of stay cable force based on measured cable shape using laser sanning", *China Journal of Highway and Transport*, vol. 34, no. 12, pp. 91–103, 2021, doi: 10.19721/j.cnki.1001-7372.2021.12.008.

[8] A.Z.Q. Al-Hijazeen, M. Fawad, M. Gerges, K. Koris, M. Salamak, "Implementation of digital twin and support vectormachine in structural health monitoring of bridges", *Archives of Civil Engineering*, vol. 69, no. 3, pp. 31–47, 2023, doi: 10.24425/ace.2023.146065.

[9] M.A. Mousa, M.M. Yussof, L.N. Assi, and S.A. Ghahari, "A pre-process enhanced digital image correlation approach for smart structure monitoring", *Infrastructures*, vol. 7, no. 10, art. no. 141, 2022, doi: 10.3390/infrastructures7100141.

[10] X. Ye and C. Dong, "Review of computer vision-based structural displacement monitoring", *China Journal of Highway and Transport*, vol. 32, no. 11, pp. 21–39, 2019, doi: 10.19721/j.cnki.1001-7372.2019.11.002.

[11] X. Shao, Y. Dai, X. He, H.T. Wang, and G. Wu, "Real-time digital image correlation for quasi-static test in civil engineering", *Acta Optica Sinica*, vol. 35, no. 10, 2015, doi: 10.3788/AOS201535.1012003.

[12] B.F. Spencer Jr., V. Hoskere, and Y. Narazaki, "Advances in computer vision-based civil infrastrtcture inspection and monitoring", *Engineering*, vol. 5, no. 2, pp. 199–222, 2019, doi: 10.1016/j.eng.2018.11.030.

[13] H.C. Jo, S.H. Kim, J. Lee, H. Sohn, and Y. Lim, "Sag-based cable tension force evaluation of cable-stayed bridges using multiple digital images", *Measurement*, vol. 186, art. no. 110053, 2021, doi: 10.1016/j.measurement.2021.110053.

[14] S. Yu, J. Zhang, and X. He, "An advanced vision-based deformation measurement method and application on a long-span cable-stayed bridge", *Measurement Science and Technology*, vol. 31, no. 6, art. no. 065201, 2020, doi: 10.1088/1361-6501/ab72c8.

[15] H.J. Lee, "Study on the efficient application of vision-based displacement measurements for the cable tension estimation of cable-stayed bridges", *Journal of the Korea Academia-Industrial Cooperation Society*, vol. 17, no. 9, pp. 709–717, 2016, doi: 10.5762/KAIS.2016.17.9.709.

[16] S.W. Kim, B. Jeon, N. Kim, and J. Park, "Vision-based monitoring system for evaluating cable tensile forces on a cable-stayed bridge," *Stuctural Health Monitoring*, vol. 12, no. 5-6, pp. 440–456, 2013, doi: 10.1177/1475921713500513.

[17] W. Du, D. Lei, P. Bai, F. Zhu, and Z. Huang, "Dynamic measurement of stay-cable force using digital image techniques", *Measurement*, vol. 151, art. no. 107211, 2020, doi: 10.1016/j.measurement.2019.107211.

[18] J. Ge, M. Su, and W. Li, "A new method for measuring cable tension of cable-stayed bridge-cable sag method", *China Railway Science*, vol. 39, no. 4, pp. 63–70, 2018, doi: 10.3969/j.issn.1001-4632.2018.04.10.

[19] H.X. Zhao, W.M. Zhang, and X.F. Jiang, "Calculation method of equivalent elastic modulus of stay cable sag effect based on catenary", *Journal of China and Foreign Highway*, vol. 40, no. 2, pp. 62–66, 2020, doi: 10.14048/j.issn.1671-2579.2020.02.013.

[20] B.F. Spencer, V. Hoskere, and Y. Narazaki, "Advances in Computer Vision-Based Civil Infrastructure Inspection and Monitoring", *Engineering*, vol. 5, no. 2, pp. 199–222, 2019, doi: 10.1016/j.eng.2018.11.030.

[21] Z. Zhang, "A flexible new technique for camera calibration," *IEEE Transactions on Pattern Analysis and Machine Intelligence*, vol. 22, no. 11, pp. 1330–1334, 2000, doi: 10.1109/34.888718.

[22] Y. Xu, J. Brownjohn, and D. Kong, "A non-contact vision-based system for multipoint displacement monitoring in a cable-stayed footbridge", *Structural Control and Health Monitoring*, vol. 25, art. no. e2155, 2018, doi: 10.1002/stc.2155.

Received: 2023-08-29, Revised: 2024-02-27